PERGAMON

International Journal of Heat and Mass Transfer 44 (2001) 2633–2642

International Journal of HEAT and MASS TRANSFER

www.elsevier.com/locate/ijhmt

A hydrodynamic and thermodynamic simulation of droplet impacts on hot surfaces, Part I: theoretical model

Dalton J.E. Harvie, David F. Fletcher *

Department of Chemical Engineering, University of Sydney, Sydney, NSW 2006, Australia

Received 13 January 2000; received in revised form 18 September 2000

Abstract

A model is presented to simulate the behaviour of an axisymmetric volatile liquid droplet impacting on a hot solid surface in the film boiling region. A volume of fluid (VOF) algorithm is used to model the gross deformation of the droplet. This algorithm is coupled to a separate one-dimensional algorithm used to model fluid flow within the viscous vapour layer existing between the droplet and solid surface. Heat transfer within the solid, liquid and vapour phases is solved, and a kinetic theory treatment is used to calculate conditions existing at the non-equilibrium interfaces of the vapour layer.

Keywords: Film boiling; Droplet impacts; Volume of fluid (VOF); Leidenfrost; Spray cooling

1. Introduction

While the interaction between liquid sprays and hot solid objects occurs in a wide variety of industrial, domestic and environmental applications, our understanding of the mechanisms involved in the process are far from complete. Indeed, current methods of estimating the heat transfer and fluid dynamics of sprays impacting hot surfaces are largely empirically derived. Of fundamental importance to such processes is the hydrodynamic and thermodynamic behaviour of individual droplets which impact a solid surface.

As a droplet nears a hot solid surface, heat is transferred from the solid to the liquid phase by the processes of conduction, convection and radiation. This energy can be used to increase the temperature of the liquid, or alternatively to vaporise liquid from the base of the droplet. If the heat transfer rate is large enough during an impact, liquid vaporised from the base of the droplet can form a 'cushion' of vapour between the solid and liquid phases, which may be capable of repelling the droplet from the solid surface. If during such an impact no direct contact between the liquid and solid phases occurs, the impact is said to be a film boiling impact. The simulation of these impacts is the subject of this study.

The temperature of a droplet prior to impacting with a solid surface may be equal to the saturation temperature corresponding to atmospheric pressure, or a temperature less than the saturation temperature. Impacts of these types are known as saturated and subcooled impacts, respectively. The model presented in this work is applicable to both types of droplet impact.

Past studies on film boiling droplet impacts have largely been empirically based, with the notable exceptions of studies by Buyevich et al. [1,2] and Inada and Yang [3]. The Buyevich et al. studies presented a film boiling impact model which assumed the droplet to be in the form of a constant volume but variable radius cylinder. Heat transfer within the vapour layer was modelled, while heat transfer within the liquid and solid phases was neglected. The droplet was assumed to be at the saturation temperature corresponding to atmospheric pressure at all times during the impact.

A comparison of a droplet impact simulated by the Buyevich *et al.* model against a documented experimental droplet impact has shown that the model does not reproduce either the dynamics or heat transfer

* Corresponding author. Tel.: +61-2-9351-4147; fax: +61-2-9351-2854.

E-mail address: davidf@chem.eng.usyd.edu.au (D.F. Fletcher).

0017-9310/01/$ - see front matter
PII: S0017-9310(00)00303-3

Nomenclature

c_p	specific heat at constant pressure (J/kg K)
F	volume of fluid (VOF) function
Gr	Grashof number
H	enthalpy (J/kg)
J	mass flux (kg/s)
k	thermal conductivity (W/m K)
Kn	Knudsen number
M	molecular mass (kg/kmol)
Ma	Marangoni number
P	pressure (Pa)
q	energy flux (W/m^2)
r	radial displacement (m)
R	universal gas constant (J/kmol K)
Re	Reynolds number
S	vapour mixture volume flowrate (m^3/s)
t	time (s)
T	temperature (K)
u	horizontal or radial velocity (m/s)
v	axial or vertical velocity (m/s)
$\dot{w}$	droplet underside vaporisation velocity (m/s)
y	vapour volume fraction
z	axial displacement (m)

Greek symbols

α	thermal diffusivity (m^2/s)
γ	ratio of specific heats
δ	vapour layer height (m)
λ	mean free path (m)
μ	absolute viscosity (N s/m^2)
ν	kinematic viscosity (m^2/s)
ρ	density (kg/m^3)
σ_t	thermal accommodation coefficient
σ_v	specular reflection coefficient

Subscripts

a	air
i	initial
l	liquid
m	vapour mixture
s	solid
v	vapour

characteristics of actual impacts [4]. It was demonstrated by Harvie that the Buyevich et al. model is unsuccessful because the cylindrical droplet form assumed is not able to reproduce the continuous deformation of an actual droplet as it approaches a solid surface. As the Inada and Yang model also assumes that the droplet form is cylindrical, and uses similar thermal assumptions to the Buyevich et al. model, similar conclusions regarding the validity of the Inada and Yang model can be drawn [4].

Fujimoto and Hatta [5] have simulated the basic hydrodynamics of transition boiling droplet impingement using a single phase two-dimensional MAC-type solution method. In their study, the droplet was assumed to contact the solid surface during the expansion phase of the impact, but in the later half of the impact when the droplet began to recollect, they assumed that a vapour layer formed beneath the droplet. Computationally, these assumptions were implemented using first a no-slip boundary condition at the lower surface of the droplet, followed by a slip boundary condition. Several impacts of water droplets whose initial diameter was less than 0.5 mm were simulated, and the hydrodynamic comparison against previously performed experimental impacts [6] was reasonable.

Other droplet impact models include the semi-empirical transition impact boiling models of Bolle and Moureau [7] and Toda [8], and the analytical nucleate boiling model of Savic [9]. Droplet impact and spreading under isothermal conditions has been simulated previously by Harlow and Shannon [10], Hatta et al. [11] and Rieber and Frohn [12], amongst others. The simulation of droplet impact and subsequent solidification has been studied by numerous researchers – further details can be found in [13].

A greater number of analytical droplet studies have been concerned with the Leidenfrost phenomenon, or steady-state droplet film boiling. Such studies include those by Gottfried et al. [14], Wachters et al. [15], Sen and Law [16], Nguyen and Avedisian [17] and Zhang and Gogos [18]. These studies generally assume a geometrical form for the evaporating droplet, and in a similar fashion to the model presented here, determine the pressures existing within the vapour layer by solving the Navier–Stokes equations. These studies have been successful in predicting droplet heat transfer rates and droplet evaporation times, especially for small diameter droplets where the droplet form is stable and nearly spherical.

This paper forms the first of two papers on the subject of film boiling droplet impacts. In this paper, the theory and assumptions used in the development of an impact model are presented. In Part II, simulations of droplet impacts are compared against real droplet impacts, to validate the impact model, and also to examine aspects of this film boiling process [19].

The droplet impact model presented in this work is composed of two main parts. To model the gross movement of the liquid droplet, a volume of fluid (VOF) fluid dynamics model has been developed. To model the behaviour of the vapour between the liquid and solid phases, and to model the heat transfer occurring within the solid, liquid and vapour phases, a separate fluid dynamics model has been developed, termed the vapour layer model. The computational coding used to execute

these two models is called 'BOUNCE'. In this study we will detail firstly the VOF algorithm, followed by the vapour layer algorithm.

2. The volume of fluid droplet code

The BOUNCE VOF code is based on the well-documented SOLA-VOF code of Nichols et al. [20], however the algorithm has been extensively modified to reflect advances that have been made in computational free surface flows over the past two decades.

The BOUNCE VOF code solves the full incompressible Navier–Stokes equations on an orthogonal cylindrical two-dimensional mesh. Momentum advection and viscous stress terms are treated implicitly, using an iterative solution procedure [4], and the momentum advection terms are evaluated using a linear combination of upwind and central differencing [20]. The continuity and momentum equations are combined to form the so-called Pressure Poisson Equation, which is solved throughout the computational domain using an Incomplete Cholesky Conjugate Gradient (ICCG) inversion algorithm [21,22].

The location of the droplet-free surface is calculated using a volume of fluid (VOF) method [20]. Under this method, a VOF function is defined which has the value of one within the droplet, and zero in the surrounding atmosphere. As the VOF function does not vary in a continuous fashion between fluid phases, advection of the function requires a special technique. The technique chosen for these simulations was that of the Defined Donating Region VOF advection algorithm [4,23], this being a volume conservative algorithm ideally suited to computationally expensive problems which require both high spatial accuracy and advection stability.

Surface tension is applied using the Continuum Surface Model (CSF) model of Brackbill et al. [24]. Under this method surface tension surface forces are replaced by surface tension volume forces, which act in a small number of computational cells surrounding the free surface interface transition region. Surface curvatures are calculated using the method outlined by Kothe et al. [21], with a correction included to account for the position of the actual fluid interface relative to the cell in which the force is applied [4]. The surface tension coefficient is assumed to be constant and equal to the coefficient evaluated at the initial temperature of the fluid.

The pressure force resulting from the viscous vapour layer, which is calculated by the separate vapour layer code, is applied using an interface region surface force [4]. The method of application is analogous to the method used to apply the surface tension force, although the vapour layer force is applied only to the lower surface of the droplet.

3. Viscous vapour layer code

Flow within the vapour layer is calculated using a computational code separate to the main droplet dynamics VOF code. Specifically, this is because the dimensions of the vapour layer are several orders of magnitude smaller than the dimensions of the droplet, and as a result, attempting to use the same computational mesh for both would result in an impractically expensive computational code. Also, by developing a new code for the viscous vapour layer, model assumptions specific to the layer can be employed, thus allowing greater efficiency and flexibility of the code compared with more standard fluid dynamics algorithms.

3.1. Theory and assumptions

Fig. 1 shows the basic variables used to analyse the viscous vapour layer. The problem is defined in two-dimensional cylindrical coordinates, with r representing the radial direction and z the vertical or axial direction. The droplet is separated from the solid surface by a distance δ, which is a function of r. The vapour has velocity components u and v in the r and z directions, respectively.

The atmosphere surrounding the droplet is assumed to contain a mixture of the vapour form of the droplet liquid, and air, with the initial proportions chosen so that the atmosphere is saturated with droplet vapour. Thus, a droplet held in the assumed atmosphere and away from any hot solid surface would not change in volume, and a droplet initially heated to saturation temperature corresponding to atmospheric pressure would be surrounded by an atmosphere containing only droplet vapour.

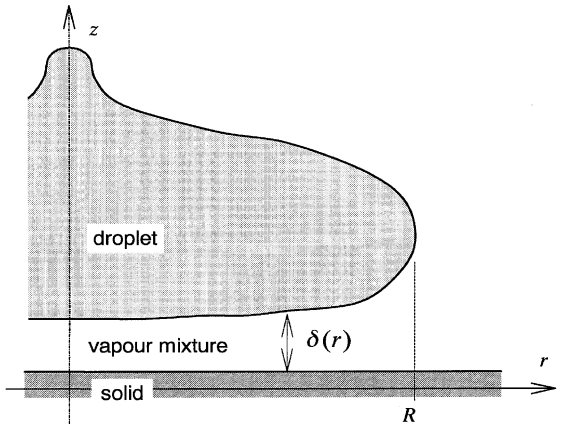

Fig. 1. The basic variables used in the viscous vapour layer analysis.

Both in the analysis and computational solution procedure, the vapour layer problem is divided into two sections:

1. *Viscous vapour flow*. Here a solution for the vapour volume fractions, fluid velocities and pressures existing beneath the droplet is found by solving a simplified form of the Navier–Stokes equations within the vapour layer. Required for this procedure is a knowledge of the position of the droplet, provided by the internal droplet dynamics VOF algorithm, and a knowledge of the droplet vaporisation velocity, $\dot{w}(r)$.
2. *Droplet vaporisation velocity*, $\dot{w}(r)$. The droplet vaporisation velocity is the velocity at which vapour is being produced at the lower surface of the droplet. This velocity is calculated by performing a heat transfer analysis within the solid, vapour mixture and liquid mediums.

In this section we outline the viscous vapour flow model, followed by the droplet vaporisation velocity model.

3.1.1. Viscous vapour flow model

3.1.1.1. Momentum conservation. In two-dimensional cylindrical coordinates, the Navier–Stokes momentum equations for incompressible Newtonian flow with gravitational terms neglected reduce to

$$\frac{\partial u}{\partial t}+u\frac{\partial u}{\partial r}+v\frac{\partial u}{\partial z}=-\frac{1}{\rho_m}\frac{\partial P}{\partial r}+\nu_m\left(\frac{1}{r}\frac{\partial}{\partial r}\left(r\frac{\partial u}{\partial r}\right)-\frac{u}{r^2}+\frac{\partial^2 u}{\partial z^2}\right) \tag{1}$$

in the radial direction, and in the vertical direction,

$$\frac{\partial v}{\partial t}+u\frac{\partial v}{\partial r}+v\frac{\partial v}{\partial z}=-\frac{1}{\rho_m}\frac{\partial P}{\partial z}+\nu_m\left(\frac{1}{r}\frac{\partial}{\partial r}\left(r\frac{\partial v}{\partial r}\right)+\frac{\partial^2 v}{\partial z^2}\right), \tag{2}$$

where the subscript m refers to vapour mixture properties, and the kinematic viscosity, ν_m, has been assumed to be constant.

In obtaining a flow solution to the momentum equations, we note that the most significant processes, in terms of repelling the droplet from the solid surface, occur when the droplet is close to the solid surface. Under such conditions, we can employ the following three assumptions:

1. the height of the vapour layer is small compared with the radius of the droplet or vapour layer;
2. the height of the layer changes slowly in the radial direction; and
3. the height of the layer changes at a velocity lower than the rate at which the vapour moves.

Using these assumptions we find that the magnitude of the vertical vapour velocity is much smaller than that of the radial velocity, and Eq. (2) simplifies to,

$$-\frac{1}{\rho_m}\frac{\partial P}{\partial z}=0. \tag{3}$$

Thus, the pressure is uniform across the height of the vapour layer. Also, in the radial direction we find that the magnitudes of the temporal, advection and radial viscous terms are all small, and the radial momentum Eq. (1) reduces to the viscous flow equation,

$$\frac{\partial^2 u}{\partial z^2}(r,z)=\frac{1}{\mu_m}\frac{\mathrm{d}P}{\mathrm{d}r}(r). \tag{4}$$

An order of magnitude analysis that was performed on Eqs. (1) and (2) during an actual droplet simulation confirmed the validity of Eqs. (3) and (4) [4].

To integrate Eq. (4) we require boundary conditions for the vapour velocity at the upper and lower surfaces of the viscous layer. In this study, the Knudsen number (Kn) is defined as the ratio of the average mean free path of the vapour mixture to the height of the vapour layer. As is shown in [19], this number can approach values of the order of 0.1 during droplet impact simulations. At these levels, the continuum assumption for the gas is justified at several mean free paths away from any adjoining medium, but a kinetic theory slip treatment must be used to model gas behaviour in regions close to any vapour interface [25,4].

A full kinetic momentum analysis of molecule behaviour at vapour interfaces is presented in [4]. The conclusion of this analysis is that an effective slip velocity can be used to model interaction between the vapour and each adjacent medium, and that the magnitude of this slip velocity, u_s, is given by

$$u_s=\left|\lambda\left(\frac{2-\sigma_v}{\sigma_v}\right)\frac{\mathrm{d}u}{\mathrm{d}z}\right|, \tag{5}$$

where λ is the average mean free path of the vapour mixture in the vicinity of the interface and σ_v is the Specular Reflection Coefficient for the combination of vapour mixture and interface material [25].

Applying Eq. (5) to both upper and lower interfaces of the vapour layer gives the slip velocities at the solid–vapour and liquid–vapour interfaces as

$$u(r,0)=\theta_s\frac{\partial u}{\partial z}(r,0)$$
$$\text{and}\quad u(r,\delta)-u_l(r)=-\theta_l\frac{\partial u}{\partial z}(r,\delta), \tag{6}$$

respectively, where u_l is defined as the radial velocity of the lower surface of the droplet as calculated by the VOF algorithm, and the variables

$$\theta_s=\frac{2-\sigma_{v,s}}{\sigma_{v,s}}\lambda_s\quad\text{and}\quad\theta_l=\frac{2-\sigma_{v,l}}{\sigma_{v,l}}\lambda_l, \tag{7}$$

have been defined. Note that the subscripts l and s in these equations indicate that properties are evaluated in

the vicinity of the liquid–vapour and solid–vapour interfaces, respectively. The viscous flow Eq. (4) can now be integrated twice in the vertical direction to yield

$$u(r,z) = \frac{1}{\mu_m}\frac{\mathrm{d}P}{\mathrm{d}r}(r)\frac{z^2}{2} + \left(\frac{z+\theta_s}{\delta+\theta_s+\theta_l}\right) \times \left[u_l(r) - \frac{\delta}{\mu_m}\frac{\mathrm{d}P}{\mathrm{d}r}(r)\left(\theta_l + \frac{\delta}{2}\right)\right]. \quad (8)$$

By averaging the vapour velocity across the height of the vapour layer, and by defining $S(r)$ to be the volume flow rate of vapour mixture within the layer, Eq. (8) can be manipulated to yield

$$S(r) = 2\pi r\delta\left\{\frac{1}{\mu_m}\frac{\mathrm{d}P}{\mathrm{d}r}(r)\left[\frac{\delta^2}{6} - \delta\frac{\left(\theta_l+\frac{\delta}{2}\right)\left(\theta_s+\frac{\delta}{2}\right)}{(\delta+\theta_l+\theta_s)}\right] + \frac{\left(\theta_s+\frac{\delta}{2}\right)}{(\delta+\theta_l+\theta_s)}u_l(r)\right\}, \quad (9)$$

which is the final form of the momentum equation used in the vapour layer flow solution.

Note that if we assume that the mean free path of the vapour mixture is large compared with the height of the vapour layer and apply a no slip velocity boundary condition, assume that the vapour layer contains only droplet vapour, and further assume that the velocity of the fluid on the underside of the droplet is zero, then Eq. (9) can be manipulated to give the average vapour layer velocity within the vapour layer as

$$\overline{u}(r) = -\frac{\delta^2}{12\mu}\frac{\partial P}{\partial r}(r). \quad (10)$$

This equation was used by Gottfried et al. [14] in their work on quasi-steady droplet evaporation, and Buyevich and Mankevich [2] in their work on droplet impacts.

3.1.1.2. Total vapour conservation. Continuity requirements within the vapour layer are solved by considering conservation of fluid volume on a cylinder of radius r', contained within the layer. Noting that the height of the vapour layer is not constant, and that vapour is produced at the lower surface of the droplet, the analysis yields the integral continuity equation [4],

$$S(r') = 2\pi\int_0^{r'}\left(\dot{w}(r) - \frac{\partial\delta}{\partial t}(r)\right)r\,\mathrm{d}r. \quad (11)$$

The differential term contained within the integral of Eq. (11) is responsible for calculating vapour volume flow rates resulting from changes in the vapour layer height. This term was not included in the analysis of Buyevich et al. [1], despite the studied problem being fully transient. The term can significantly affect droplet dynamics by increasing vapour layer pressures as the droplet nears the solid surface, and decreasing vapour layer pressures as the droplet moves away.

3.1.1.3. Vapour mixture solution. For the purposes of determining the proportions of droplet vapour and air within the vapour layer, the total vapour pressure beneath the droplet is specified by the ideal gas assumption

$$P = P_v + P_a, \quad (12)$$

where P_v is the partial droplet vapour pressure, and P_a is the partial air pressure.

BOUNCE uses an incompressible gas assumption when solving the Navier–Stokes equations, but an ideal gas assumption when determining the vapour layer constitution. Incompressible flow within the vapour layer has been assumed when solving the momentum equations because total gauge pressures generated within the vapour layer are small compared with atmospheric pressure, so variations in constituent vapour densities within the layer are only small.

Utilising Eq. (12), and assuming that the gases are well mixed across the small height of the vapour layer, the volume fractions of air and droplet vapour within the layer can be expressed as, respectively,

$$y_a(r) = \frac{P_a(r)}{P(r)} \quad \text{and} \quad y_v(r) = \frac{P_v(r)}{P(r)} = 1 - y_a(r). \quad (13)$$

The vapour layer density is given by,

$$\rho_m(r) = y_a(r)\rho_a + (1 - y_a(r))\rho_v, \quad (14)$$

where the air density, ρ_a, and droplet vapour density, ρ_v, are determined at atmospheric pressure and at the average vapour layer temperature of

$$T_v = \frac{T_{s,i} + T_{sat}(P_{atmos})}{2}. \quad (15)$$

The vapour layer thermal conductivity, k_m, and vapour layer dynamic viscosity, μ_m are defined similarly.

To determine the volume fraction of air within the vapour layer, a conservation analysis similar to that presented in the previous section is used, yielding the integral transport equation [4],

$$y_a(r') = \frac{-2\pi}{S(r')}\int_0^{r'}\left(y_a(r)\frac{\mathrm{d}\delta(r)}{\mathrm{d}t} + \delta(r)\frac{\mathrm{d}y_a(r)}{\mathrm{d}t}\right)r\,\mathrm{d}r. \quad (16)$$

The initial air volume fraction is determined by assuming that the atmosphere surrounding the droplet is saturated and at the initial temperature of the droplet.

To determine the pressures generated within the vapour layer, Eqs. (9), (11) and (16) are solved simultaneously using an iterative solution method. Note that when integrating equation (9), the pressure at the extremity of the vapour layer is assumed to be atmospheric.

3.1.2. Droplet vaporisation velocity model

The droplet vaporisation velocity, $\dot{w}$, is defined as the velocity at which vapour is produced at the lower

surface of the droplet. In order to calculate this velocity, heat transfer rates within the solid, vapour mixture and liquid phases must be calculated.

Fig. 2 shows temperature variables defined for the vaporisation velocity calculation. Note that temperatures are dependent on r as well as z – this figure illustrates temperatures at only one radial location. The temperatures of the solid and liquid phases are represented by $T_s(r,z)$ and $T_l(r,z)$, respectively, and the initial temperatures of the solid and liquid phases are $T_{s,i}$ and $T_{l,i}$, respectively. The temperature of the solid at the solid-vapour interface is $T_{ss}(r)$, and the temperature of the vapour at the solid–vapour interface is $T_{sv}(r)$. Similarly, the temperature of the liquid at the liquid–vapour interface is $T_{ll}(r)$, and the temperature of the vapour at the liquid-vapour interface is $T_{lv}(r)$.

Also shown in Figure 2 are heat transfer rates existing at both the liquid–vapour and solid–vapour interfaces. The heat transfer rate out of the solid is q_s, the heat transfer rate into the bulk of the liquid is q_l, and the heat transfer rate across the vapour region is q_v. These heat transfer rates are all functions of r.

3.1.2.1. Solid phase heat transfer. In two-dimensional cylindrical coordinates, the heat diffusion equation describing conduction within the solid is [26],

$$\frac{\partial T}{\partial t} = \alpha_s \left[\frac{1}{r} \frac{\partial}{\partial r} \left(r \frac{\partial T}{\partial r} \right) + \frac{\partial^2 T}{\partial z^2} \right], \tag{17}$$

where a constant thermal conductivity, k_s, for the solid has been assumed. The thermal diffusivity for the solid is $\alpha_s = k_s/c_s\rho_s$, where c_s is the specific heat and ρ_s is the density of the solid.

During hot surface droplet impacts, solid temperature variations in the radial direction are typically small compared with variations in the axial direction. To illustrate this point, for solids which are examined in this study, the thermal diffusivity is typically of the order 1×10^{-5} m^2/s. For a droplet with a diameter of around 2 mm, simulations indicate that the droplet is in residence with the surface for a time period of the order of 5 ms. Thus the thermal diffusion length, conservatively defined as $\sqrt{\alpha t}$, is of the order of 0.2 mm. This length is considerably less than the diameter of the droplet. Consequently, heat transfer within the solid is dominated by conduction in the axial rather than in the radial direction, and the heat diffusion Eq. (17) can be simplified to give,

$$\frac{\partial T_s}{\partial t} = \alpha_s \frac{\partial^2 T_s}{\partial z^2}. \tag{18}$$

In order to integrate Eq. (18) to find the temperature distribution within the solid, boundary conditions are required to describe conditions at the solid–vapour interface, and within the body of the solid.

At the solid–vapour interface, the rate of heat loss to the vapour phase is given by Fourier's Law as

$$q_s(r) = -k_s \frac{\partial T_s}{\partial z}(r,0). \tag{19}$$

For the internal solid boundary condition, we assume that the solid has a thickness which is large compared with the thermal diffusion length, so that

$$T_s(r,-\infty) = T_{s,i}. \tag{20}$$

Eq. (18), combined with (Eqs. 19) and (20), and a knowledge of the heat loss rate from the solid, $q_s(r)$, provide a solution for the temperature distribution within the solid phase.

3.1.2.2. Vapour phase heat transfer. In two-dimensional cylindrical coordinates, the equation for conservation of thermal energy in an incompressible fluid, assuming constant thermal conductivity, is given as [27],

$$\begin{aligned} \frac{\partial T}{\partial t} + u\frac{\partial T}{\partial r} + v\frac{\partial T}{\partial z} = {} & \frac{k}{c_p\rho}\left[\frac{1}{r}\frac{\partial}{\partial r}\left(r\frac{\partial T}{\partial r}\right) + \frac{\partial^2 T}{\partial z^2}\right] \\ & + 2\frac{\mu}{c_p\rho}\left[\left(\frac{\partial u}{\partial r}\right)^2 + \left(\frac{u}{r}\right)^2 \right. \\ & \left. + \left(\frac{\partial v}{\partial z}\right)^2 + \frac{1}{2}\left(\frac{\partial v}{\partial r} + \frac{\partial u}{\partial z}\right)^2\right]. \end{aligned} \tag{21}$$

Eq. (21) can be greatly simplified to represent heat transfer within the vapour layer, by examining the magnitude of each of the constituent terms:

1. Using the assumptions that were made in Section 3.1.1 regarding the geometry of the vapour layer, we conclude that all terms in Eq. (21) which represent changes in the radial direction are small compared with terms representing changes in the axial direction, as the height of the vapour layer is considerably smaller than the radius of the vapour layer.
2. Comparing the convection and conduction terms in Eq. (21), the non-dimensional ratio $v\delta/\alpha_m$ is small,

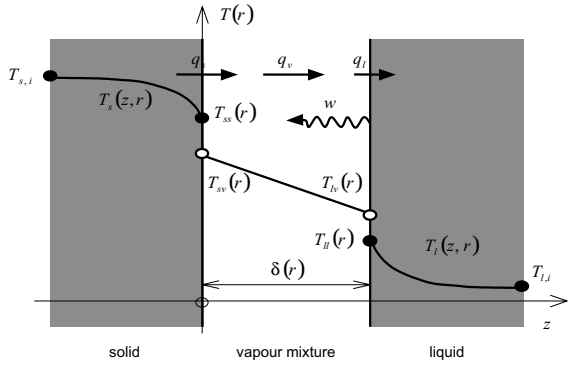

Fig. 2. Liquid, vapour mixture and solid temperatures at radius r used in the calculation of the vaporisation velocity, $\dot{w}$.

and thus, the axial convective term in Eq. (21) can be neglected.

3. Similarly, comparing the conductive and viscous generation terms in Eq. (21), we note that the thermal conductivity, k, for gases of interest in this study is several orders of magnitude larger than the absolute viscosity, μ, for these same gases. Thus, the non-dimensional ratio $2\mu u^2/kT$ is small, and consequently, the viscous dissipation terms in Eq. (21) may be neglected.
4. Finally, droplet and solid surface temperature variations in time are small compared with temperature variations across the vapour layer in the axial direction, and consequently, the temporal term in Eq. (21) can be neglected.

Utilising these assumptions, Eq. (21) reduces to the one-dimensional steady-state conduction equation,

$$\frac{\partial^2 T_v}{\partial z^2} = 0. \tag{22}$$

Integrating twice in the axial direction, using the solid surface and liquid surface temperatures as boundary conditions gives the temperature distribution within the vapour layer as

$$T_v = T_{sv} + \frac{z}{\delta}(T_{lv} - T_{sv}). \tag{23}$$

As a linear temperature distribution has been obtained, the heat transfer rate across the layer is constant, and given by

$$q_v(r) = \frac{k_m}{\delta}(T_{sv}(r) - T_{lv}(r)). \tag{24}$$

Note that heat transfer by radiation across the vapour layer has been neglected in this study. The maximum possible radiative heat loss rate by the solid surface is given by the heat loss rate from a black body at the temperature of the surface [26]. Comparing this maximum radiative heat rate to the conductive heat transfer rate across the vapour layer, we find that radiative heat transfer can be neglected below an initial solid surface temperature of approximately 700°C. Thus, this temperature defines the upper solid temperature limit for the model.

3.1.2.3. Liquid phase heat transfer. Heat transfer within the liquid phase is described by the following thermal energy transport equation for incompressible fluids represented using a VOF function in two-dimensional cylindrical coordinates [4],

$$F\frac{\partial T_l}{\partial t} + uF\frac{\partial T_l}{\partial r} + vF\frac{\partial T_l}{\partial z} = \alpha_l\left[\frac{1}{r}\frac{\partial}{\partial r}\left(rF\frac{\partial T_l}{\partial r}\right) + \frac{\partial}{\partial z}\left(F\frac{\partial T_l}{\partial z}\right)\right], \tag{25}$$

where F is the local VOF fraction. Note that for liquids commonly involved in hot surface droplet impacts, thermal energy generation by viscous dissipation is negligible, as the dimensionless parameter $2\mu u^2/kT$ is small.

As in the solid conduction analysis of Section 3.1.2.1, we evaluate the characteristic thermal diffusion time, $\sqrt{\alpha t}$, for a typical droplet liquid. The thermal diffusivity of liquids used in droplet impacts is typically of the order 2×10^{-7} m^2/s. For an approximate impact time of 5 ms for a 2 mm diameter droplet, this gives a thermal diffusion length of the order of 0.03 mm. As this diffusion length is considerably smaller than the dimensions of the droplet, we can again assume that the effect of conduction in the radial direction is negligible compared with conduction in the axial direction, and the radial conduction term in Eq. (25) can be neglected.

Eq. (25) provides a solution to the temperature distribution within the droplet in terms of absolute coordinates – coordinates that are relative to the solid surface. For the computational solution, it is more convenient to work with a combination of absolute coordinates, and coordinates which are relative to the lower surface of the droplet.

Defining a relative coordinate system using dashed variables,

$$t' = t, r' = r \quad \text{and} \quad z' = z - \delta(t, r). \tag{26}$$

Eq. (25) can be transformed to yield [4],

$$F\frac{\partial T_l}{\partial t'} + uF\frac{\partial T_l}{\partial r} + v'F\frac{\partial T_l}{\partial z'} = \alpha_l\left[F\frac{\partial^2 T_l}{\partial z'^2} + \frac{\partial F}{\partial z'}\frac{\partial T_l}{\partial z'}\right]. \tag{27}$$

The radial differential operator is not redefined in the relative coordinate system for reasons of computational simplicity.

The term $\partial F/\partial z'$ in Eq. (27) represents the gradient of the VOF function, in coordinates relative to the lower droplet surface. However, as the thermal diffusion length $\sqrt{\alpha t}$ was shown to be significantly smaller than the dimensions of the droplet, the VOF function can be assumed to be axially constant within the droplet volume in which we wish to calculate the liquid heat transfer rates. Thus, we can assume

$$\frac{\partial F}{\partial z'} = 0, \tag{28}$$

and Eq. (27) simplifies to give

$$\frac{\partial T_l}{\partial t'} + u\frac{\partial T_l}{\partial r} + v'\frac{\partial T_l}{\partial z'} = \alpha_l\frac{\partial^2 T_l}{\partial z'^2}. \tag{29}$$

In order to integrate Eq. (29), boundary conditions for heat conduction at the liquid–vapour interface and within the body of the droplet are required. At the

liquid–vapour interface, Fourier's law gives the rate of heat loss into the droplet as

$$q_{\mathrm{l}}(r) = -k_{\mathrm{l}} \frac{\partial T_{\mathrm{l}}}{\partial z'}(r,0). \tag{30}$$

As in the solid conduction analysis, the diameter of the droplet is two orders of magnitude larger than the heat diffusion length within the droplet, so that

$$T_{\mathrm{l}}(r,\infty) = T_{\mathrm{l},i}. \tag{31}$$

An adiabatic boundary condition is used at the radial extremities of the droplet.

Two forms of heat convection within the droplet have been neglected in this study; natural convection and Marangoni convection. Natural convection is convection driven by buoyant forces within the fluid. The effects of natural convection may be neglected in a heat transfer analysis when the inequality

$$\frac{Gr}{Re^2} \ll 1 \tag{32}$$

holds [26], where Re is the Reynolds number, and Gr the Grashof number. Using typical values for droplet types examined in this study, we find that the above ratio is of the order of 0.001, and we are justified in neglecting the effects of natural convection.

Marangoni convection is convection driven by changes in the magnitude of surface tension along a fluid interface. These changes may be caused by changes in the liquid temperature along a fluid interface, as the magnitude of surface tension is dependent on the temperature of a fluid. The magnitude of the force which drives such a convection is given by [28]

$$p_T = \nabla\sigma, \tag{33}$$

where p_T is the resulting pressure directed tangentially along the interface, and σ the surface tension coefficient of the liquid. Substituting in typical values for water droplets examined in this study we find that the magnitude of p_T is of the order of 10 Pa. This pressure is small compared with gauge pressures generated within the vapour layer [4], so given the short timescale over which these droplet impacts occur, it does not appear that Marangoni convection is significant in this study.

We now turn our attention to both vapour layer interfaces, where an energy balance and an examination of the conditions existing at those boundaries are made.

3.1.2.4. Solid–vapour interface. Energy balance. An energy balance at the solid–vapour interface reveals

$$q_{\mathrm{s}}(r) = q_{\mathrm{v}}(r). \tag{34}$$

Substituting Eq. (19) for the heat loss rate from the solid, and Eq. (24) for the energy transfer rate across the vapour layer, yields

$$k_{\mathrm{s}} \frac{\partial T_{\mathrm{s}}}{\partial z}(r,0) = \frac{k_m}{\delta}(T_{\mathrm{lv}}(r) - T_{\mathrm{sv}}(r)). \tag{35}$$

Interface conditions. As the Knudsen number within the vapour layer can reach values of the order of 0.1 during droplet impact simulations, the vapour flow within the viscous layer is in the slip regime, and a molecular treatment is required to describe the change in fluid velocities occurring across both the solid–vapour and liquid–vapour interfaces. In an analogous manner, the molecular slip flow regime existing within the vapour layer dictates that a molecular temperature discontinuity treatment is required to describe the variation in fluid temperature across the solid–vapour and liquid–vapour interfaces [4,25].

Following the analysis presented in Harvie [4], the relationship between temperatures existing on either side of the solid-liquid interface can be represented by

$$T_{\mathrm{ss}}(r) - T_{\mathrm{sv}}(r) = \lambda_{\mathrm{s}} \left(\frac{9\gamma - 5}{4}\right)\left(\frac{2}{\gamma\sigma_{\mathrm{t,s}}} - 1\right)\frac{\mathrm{d}T_{\mathrm{v}}}{\mathrm{d}z}(r,0), \tag{36}$$

where $\sigma_{\mathrm{t,s}}$ is the Thermal Accommodation Coefficient for the combination of vapour and solid surface. Noting that the temperature profile within the vapour is linear, as given by Eq. (23), Eq. (36) becomes

$$T_{\mathrm{sv}}(r) - T_{\mathrm{ss}}(r) = \frac{\lambda_{\mathrm{s}}}{\delta}\left(\frac{9\gamma - 5}{4}\right)\left(\frac{2}{\gamma\sigma_{\mathrm{t,s}}} - 1\right)(T_{\mathrm{lv}}(r) - T_{\mathrm{sv}}(r)) \tag{37}$$

and the conditions at the solid–vapour interface are specified.

3.1.2.5. Liquid–vapour interface. Energy balance. In a similar manner to the solid–vapour interface, an energy balance at the liquid–vapour interface reveals that

$$q_{\mathrm{v}}(r) = q_{\mathrm{l}}(r) + \dot{w}\rho_{\mathrm{v}} H_{fg,c}. \tag{38}$$

In this equation, the latent heat of vaporisation is corrected to account for the sensible heat contained within the vapour layer,

$$H_{fg,c} = H_{fg}(T_{\mathrm{sat}}(P_{\mathrm{atmos}})) + c_{\mathrm{p,v}}\left(\frac{T_{\mathrm{s},i} - T_{\mathrm{sat}}(P_{\mathrm{atmos}})}{2}\right). \tag{39}$$

Substituting Eqs. (24) and (30) into Eq. (38) gives the energy balance at the interface as

$$\frac{k_m}{\delta}(T_{\mathrm{sv}}(r) - T_{\mathrm{lv}}(r)) = -k_{\mathrm{l}}\frac{\partial T_{\mathrm{l}}}{\partial z'}(r,0) + \dot{w}\rho_{\mathrm{v}} H_{fg,c}. \tag{40}$$

Mass balance. In addition to the equations specified for the solid–vapour interface, at the liquid–vapour interface a mass balance equation is required. A molecular evaluation of evaporation and condensation rates existing at the liquid–vapour boundary yields the total vaporisation velocity at the interface as [4],

$$\dot{w} = \frac{\sigma_{t,l}}{\rho_v}\sqrt{\frac{M_v}{2\pi R}}\left(\frac{P_{sat}(T_{ll}(r))}{\sqrt{T_{ll}(r)}} - \frac{P(r)}{\sqrt{T_{lv}(r)}}\right). \quad (41)$$

Here $\sigma_{t,l}$ is the Thermal Accommodation Coefficient for the combination of liquid and vapour mixtures, M_v is the molecular weight of the droplet vapour, R the universal gas constant and P the absolute vapour pressure within the vapour layer.

Interface conditions. The magnitude of the effective temperature discontinuity at the solid–vapour interface is given by [4]

$$T_{lv}(r) - T_{ll}(r) = -\frac{\lambda_l}{\phi}\left(\frac{9\gamma - 5}{4}\right)\left(\frac{2}{\gamma\sigma_{t,l}} - 1\right)\frac{dT_v}{dz}(r,\delta). \quad (42)$$

Noting that the temperature profile within the vapour is linear, as given by Eq. (23), Eq. (42) becomes

$$T_{lv}(r) - T_{ll}(r) = -\frac{\lambda_l}{\phi\delta}\left(\frac{9\gamma - 5}{4}\right)\left(\frac{2}{\gamma\sigma_{t,l}} - 1\right) \times (T_{lv}(r) - T_{sv}(r)). \quad (43)$$

The variable ϕ is defined as the ratio of the molecular evaporation to condensation rates,

$$\phi = \frac{J_e}{J_c} = \frac{\dot{w}\rho_v\sqrt{T_{lv}(r)}}{\sigma_{t,l}P_v}\sqrt{\frac{2\pi R}{M_v}} + 1. \quad (44)$$

The droplet vaporisation velocity can now be found by the simultaneous solution of Eqs. (18), (20), (29), (31), (35), (37), (40), (41) and (43).

4. Numerical procedure

The droplet impact algorithm has been implemented using a Fortran code called BOUNCE. The vapour layer code works within the VOF code – the VOF code feeds the vapour layer code in the geometry of the droplet, from which the vapour layer code calculates pressures existing beneath the droplet. These pressures are then fed back to the VOF code to determine changes in the geometry of the droplet. As the variables passed between the VOF and vapour layer codes are treated implicitly, an iterative procedure is required to finalise end of timestep values. Further details of the procedure can be found in [4].

The film boiling impact problem is a stiff problem, meaning that it involves physical processes which operate on radically different timescales. A result of this stiffness is that droplet simulations require small timesteps, and consequently the BOUNCE code is quite computationally expensive. Typically the simulation of a complete droplet impact requires of the order of 10,000 timesteps, which corresponds to several hours of computation on a 200 MHz Pentium PC.

5. Conclusions

A new droplet impact model that is capable of modelling the impact of non-saturated droplets on hot surfaces in the film boiling regime has been presented. The model uses a VOF algorithm to simulate the gross droplet deformation, and a separate one-dimensional fluid algorithm to simulate vapour flow within the viscous vapour layer. Heat transfer within the solid, liquid and vapour phases is solved, and a molecular interface treatment is used to describe the non-equilibrium conditions existing at the vapour region boundaries. Validation of the model is accomplished in a companion paper [19], where simulated droplet impacts are compared with documented actual droplet impacts.

References

[1] Y.A. Buyevich, V.N. Mankevich, M.I. Polotsky, Toward the theory of fall of a droplet onto an overheated surface, Teplofiz. Vysok. Temp. 24 (1986) 743–752 1986.
[2] Y.A. Buyevich, V.N. Mankevich, Interaction of a dilute mist flow with a hot body, Int. J. Heat Mass Transfer 38 (1995) 731–744.
[3] S. Inada, W.J. Yang, Film boiling heat transfer for saturated drops impinging on a heated surface, Int. J. Heat Mass Transfer 37 (1994) 2588–2591.
[4] D.J.E. Harvie, A hydrodynamic and thermodynamic simulation of droplet impacts on hot surfaces, Ph.D. Thesis, Department of Mechanical and Mechatronic Engineering, University of Sydney, NSW, Australia, 1999.
[5] H. Fujimoto, N. Hata, Deformation and rebounding processes of a water droplet impinging on a flat surface above Leidenfrost temperature, J. Fluids Eng. 118 (1996) 142–149.
[6] N. Hatta, H. Fujimoto, H. Takuda, K. Kinoshita, O. Takahashi, Collision dynamics of a water droplet impinging on a rigid surface above the Leidenfrost temperature, ISIJ Int. 35 (1995) 50–55.
[7] L. Bolle, J.C. Moureau, Spray cooling of hot surfaces, Multiphase Sci. Technol. 1 (1976) 1–92.
[8] S. Toda, Study of mist cooling (first report: investigation of mist cooling). Heat Transfer, Japanese Res., 1 (1972) 39–50.
[9] P. Savic, The cooling of a hot surface by drops boiling in contact with it. Technical Report MT-37, National Research Council of Canada, Ottawa, April 1958.
[10] F.H. Harlow, J.P. Shannon, The splash of a liquid drop, J. Appl. Phys. 38 (1967) 3855–3866.
[11] N. Hatta, H. Fujimoto, H. Takuda, Deformation process of a water droplet impinging on a solid surface, J. Fluids Eng. 117 (1995) 394–401.
[12] M. Rieber, A. Frohn, A numerical study on the mechanism of splashing, Int. J. Heat Fluid Flow 20 (1999) 455–461.
[13] E.J. Lavernia,Y. Wu, Spray Atomization and Deposition. Wiley, West Sussex, England, 1996.
[14] B.S. Gottfried, C.J. Lee, K.J. Bell, The Leidenfrost phenomenon: film boiling of liquid droplets on a flat plate, Int. J. Heat Mass Transfer 9 (1966) 1167–1187.

[15] L.H.J. Wachters, L. Smulders, J.R. Vermeulen, H.C. Kleiweg, The heat transfer from a hot wall to impinging mist droplets in the spheroidal state, Chem. Eng. Sci. 21 (1966) 1231–1238.
[16] A.K. Sen, C.K. Law, On a slowly evaporating droplet near a hot plate, Int. J. Heat Mass Transfer 27 (1984) 1418–1421.
[17] T.K. Nguyen, C.T. Avedisian, Numerical solution for film evaporation of a spherical droplet on an isothermal and adiabatic surface, Int. J. Heat Mass Transfer 30 (1987) 1497–1509.
[18] S. Zhang, G. Gogos, Film evaporation of a spherical droplet over a hot surface: fluid mechanics and heat/mass transfer analysis, J. Fluid Mech. 222 (1991) 543–563.
[19] D.J.E. Harvie, D.F. Fletcher, A hydrodynamic and thermodynamic simulation of droplet impacts on hot surfaces, Part II: validation and applications, Int. J. Heat Mass Transfer 44 (2001) 2643–2659.
[20] B.D. Nichols, C.W. Hirt, R.S. Hotchkiss, SOLA-VOF: a solution algorithm for transient fluid flow with multiple free boundaries, Technical Report LA-8355, Los Alamos Scientific Laboratory, August 1980.
[21] D.B. Kothe, R.C. Mjolsness, M.D. Torrey, RIPPLE: a computer program for incompressible flows with free surfaces, Technical Report LA-12007-MS, Los Alamos National Laboratory, October 1994.
[22] D.S. Kershaw, The Incomplete Cholesky-Conjugate Gradient method for the iterative solution of systems of linear equations, J. Comput. Phys. 26 (1978) 43–65.
[23] D.J.E. Harvie, D.F. Fletcher, A new volume of fluid advection algorithm: the defined donating region scheme, Int. J. Numer. Meth. Fluids 35 (2001) 151–172.
[24] J.U. Brackbill, D.B. Kothe, C. Zemach, A continuum method for modeling surface tension, J. Comput. Phys. 100 (1992) 335–354.
[25] W.M. Rohsenow, H.Choi, Heat, Mass and Momentum Transfer, Prentice-Hall, 1961.
[26] F.P. Incropera, D.P. DeWitt, Fundamentals of Heat and Mass Transfer, fourth ed., Wiley, New York, 1996.
[27] R.B. Bird, W.E. Stewart, E.N. Lightfoot, Transport Phenomena, Wiley, New York, 1960.
[28] J.C. Legros, O. Dupont, P. Queeckers, S. VanVaerenbergh, D. Schwabe, Thermohydrodynamic instabilities and capillary flows, Low-Gravity Fluid Dynamics and Transport Phenomena – Prog. Astronaut. Aeronaut. 130 (1990) 207–239.